

Conditioning of a Hybrid High-Order scheme on meshes with small faces

Santiago Badia¹, Jérôme Droniou², and Liam Yemm³

¹School of Mathematics, Monash University, Melbourne, Australia, santiago.badia@monash.edu

²School of Mathematics, Monash University, Melbourne, Australia, jerome.droniou@monash.edu

³School of Mathematics, Monash University, Melbourne, Australia, liam.yemm@monash.edu

Abstract

We conduct a condition number analysis of a Hybrid High-Order (HHO) scheme for the Poisson problem. We find the condition number of the statically condensed system to be independent of the number of faces in each element, or the relative size between an element and its faces. The dependence of the condition number on the polynomial degree is tracked. Next, we consider HHO schemes on unfitted meshes. It is well known that the linear systems obtained on unfitted meshes can be arbitrarily ill-conditioned due to the presence of sliver-cut and small-cut elements. We show that the condition number arising from HHO schemes on such meshes is not as negatively effected as those arising from conforming methods. We describe how the condition number can be improved by aggregating ill-conditioned elements with their neighbours.

Key words: Hybrid High-Order methods, condition number, small faces.

MSC2010: 65N12, 65N15, 65N30.

1 Introduction

Several hybrid discretisation methods have been proposed in recent years for the numerical discretisation of partial differential equations [17, 5, 13]. One of the selling points of these schemes is their geometrical flexibility. Discretisation spaces are not bound to specific element topologies and can readily be used on general polytopal meshes. Body-fitted unstructured mesh generation is one of the main bottlenecks in complex numerical simulations, which requires intensive human intervention. Usually, these meshes are composed of tetrahedral (and/or hexahedral) elements. Polytopal methods can provide sought-after flexibility in the mesh generation step.

In this work, we focus on the hybrid high order (HHO) method. Developed in [17, 16], the HHO method is a modern polytopal method for elliptic PDEs. A key aspect of HHO is its applicability to generic meshes with arbitrarily shaped elements. Additionally, HHO methods are of arbitrary order, dimension independent, and are amenable to static condensation. We refer the reader to [15] for a thorough review of the method and its applications. An analysis on skewed meshes has been carried out for a diffusion problem in [19] and identifies how the error estimate is impacted by the element distortion and local diffusion tensor. The recent work of [20] shows the HHO method to be accurate on meshes possessing elements with arbitrarily many small faces.

Unfitted (a.k.a. embedded and immersed) discretisations can also simplify the geometrical discretisation step. The domain of interest is embedded in a simple background mesh (e.g., a Cartesian grid). The boundary (or interface) treatment is tackled at the numerical integration

and discretisation step. Many unfitted finite element (FE) schemes that rely on a standard FE space on the background mesh have been proposed; see, e.g. the extended finite element method (XFEM) [6], the cutFEM method [9], the aggregated finite element method (FEM) [4], the finite cell method [26] and discontinuous Galerkin (DG) methods with element aggregation [23].

Unfitted formulations can produce arbitrarily ill-conditioned linear systems [14]. The intersection of a background element with the physical domain can be arbitrarily small and with an unbounded aspect ratio. It is known as the *small cut element problem*. This problem is also present on unfitted interfaces with a high contrast of physical properties [25]. Few unfitted formulations are fully robust and optimal regardless of cut location or material contrast. The ill-conditioning issue was addressed in [7] via the so-called ghost penalty stabilisation. Instead of adding stabilisation terms, the small cut element problem can be fixed by element aggregation (or agglomeration). This approach has been proposed in [23] for DG methods. While aggregation is natural in DG methods (these schemes can readily be used on polytopal meshes), its extension to conforming spaces is more involved. The design of well-posed C^0 Lagrangian finite elements on agglomerated meshes has been proposed in [4]. The aggregated FEM constructs a discrete extension operator from well-posed to ill-posed degrees of freedom that preserves continuity. All these formulations enjoy good numerical properties, such as stability, condition number bounds, optimal convergence and continuity with respect to data.

The FE discretisation of linear second-order elliptic operators (e.g. the Laplacian) in weak form produces linear systems such that the ℓ^2 -condition number (on shape regular, quasi-uniform meshes) scales as the inverse square of the mesh size [21]. We refer to [12] for the condition number analysis of hybridised DG methods on regular simplicial quasi-uniform meshes. The authors in [24] investigate experimentally the ill-conditioning of the virtual element methods for high-order bases on distorted meshes. In this work, we analyse the properties of the linear systems that arise from HHO formulations. We prove estimates for the condition number arising from such systems. We show that the estimates remain robust with respect to small element faces and track the dependence in the estimates of the polynomial degree of the unknowns. The linear systems in HHO methods are obtained after the static condensation of the element unknowns. This process allows the global system to depend only on the face unknowns [15, Appendix B.3.2]. In Section 2.2.3 we state some estimates on the spectrum and conditioning of this condensed operator. We find that if each face is attached to at least one element of diameter comparable to the mesh size, then the condition number scales as $h_{\min}^{-1} h_{\max}^{-1}$ (where h_{\min} and h_{\max} respectively denote the minimum and maximum element diameters in the mesh). We note this is a potentially significantly better estimate than h_{\min}^{-2} for FEM or DG. To the best of our knowledge, no condition number estimates on general meshes exist for HHO or virtual element methods.

Next, we apply the HHO method on unfitted meshes. The analysis tells us the potential conditioning issues of HHO schemes on such meshes, for which arbitrarily small elements (and faces) appear scattered among large elements [8]. Based on the analysis, we know that we must aggregate highly distorted small cut elements (e.g., due to sliver cuts) to interior elements. Since arbitrary small faces do not affect condition number bounds, there is no need for face aggregation or stabilisation. This way, we end up with an unfitted HHO method that leads to well-posed linear systems and optimal condition numbers.

Unfitted hybrid methods have some benefits compared to more standard unfitted FEs. First, we can enforce Dirichlet boundary conditions strongly; there are degrees of freedom located on boundaries faces. In unfitted standard FEs, degrees of freedom are defined in the background mesh. Dirichlet boundary conditions and trace continuity on interfaces are weakly enforced (using, e.g., Nitsche's method [22]). Second, the method does not involve the tuning of additional stabilisation parameters, which can have an impact on results [2]. Third, the extension to high

order is straightforward. It is more complicated in face-based ghost penalty (it involves penalty terms on jumps of high-order derivatives) [7] or aggregated FEs (extension operators for high order can amplify rounding errors) [4].

The remainder of this paper is organised as follows: In Section 2 we introduce the HHO method and state our key findings. In Section 3 we prove the results, and in Section 5 we conduct a thorough numerical analysis of the condition number on various meshes.

2 Presentation of the HHO method and main result

2.1 Model problem

We take a polytopal domain $\Omega \subset \mathbb{R}^d$, $d \geq 2$ and a source term $f \in L^2(\Omega)$, and consider the Dirichlet problem: Find u such that

$$\begin{aligned} -\Delta u &= f & \text{in } \Omega \\ u &= 0 & \text{on } \partial\Omega. \end{aligned}$$

The variational problem reads: find $u \in H_0^1(\Omega)$ such that

$$a(u, v) = \mathcal{L}(v), \quad \forall v \in H_0^1(\Omega), \quad (2.1)$$

where $a(u, v) := (\nabla u, \nabla v)_\Omega$ and $\mathcal{L}(v) := (f, v)_\Omega$. Here and in the following, $(\cdot, \cdot)_X$ is the L^2 -inner product of scalar- or vector-valued functions on a set X for its natural measure.

2.2 HHO scheme

Let $\mathcal{H} \subset (0, \infty)$ be a countable set of mesh sizes with a unique cluster point at 0. For each $h \in \mathcal{H}$, we partition the domain Ω into a mesh $\mathcal{M}_h = (\mathcal{T}_h, \mathcal{F}_h)$, for which a detailed definition can be found in [15, Definition 1.4]. The set of mesh elements \mathcal{T}_h is a disjoint set of polytopes such that $\bar{\Omega} = \bigcup_{T \in \mathcal{T}_h} \bar{T}$. The set \mathcal{F}_h is a collection of mesh faces forming a partition of the mesh skeleton, i.e. $\bigcup_{T \in \mathcal{T}_h} \partial T = \bigcup_{F \in \mathcal{F}_h} \bar{F}$. The boundary faces $F \subset \partial\Omega$ are gathered in the set \mathcal{F}_h^b . The parameter h is given by $h := \max_{T \in \mathcal{T}_h} h_T$ where, for $X = T \in \mathcal{T}_h$ or $X = F \in \mathcal{F}_h$, h_X denotes the diameter of X . We shall also collect the set of faces attached to an element $T \in \mathcal{T}_h$ in the set $\mathcal{F}_T := \{F \in \mathcal{F}_h : F \subset T\}$. The (constant) unit normal to $F \in \mathcal{F}_T$ pointing outside T is denoted by \mathbf{n}_{TF} , and $\mathbf{n}_{\partial T} : \partial T \rightarrow \mathbb{R}^d$ is the piecewise constant outer unit normal defined by $(\mathbf{n}_{\partial T})|_F = \mathbf{n}_{TF}$ for all $F \in \mathcal{F}_T$. Throughout this work we make the following assumption on the meshes, which allows for some meshes with arbitrarily large numbers of face in each element, or faces that have an arbitrarily small diameter compared to their elements' diameters.

Assumption 1 (Regular mesh sequence). *There exists a constant $\varrho > 0$ such that, for each $h \in \mathcal{H}$, each $T \in \mathcal{T}_h$ is connected by star-shaped sets with parameter ϱ (see [15, Definition 1.41]).*

From hereon, we shall denote $f \lesssim g$ to mean $f \leq Cg$ where C is a constant depending only on Ω , d and ϱ , but independent of the considered face/element, the degrees of the considered polynomial spaces, and quantities f, g . We shall also write $f \approx g$ if $f \lesssim g$ and $g \lesssim f$. When necessary, we make some additional dependencies of the constant C explicit.

2.2.1 Local construction

Let $X = T \in \mathcal{T}_h$ or $X = F \in \mathcal{F}_h$ be a face or an element in a mesh \mathcal{M}_h , and let $\mathbb{P}^\ell(X)$ be the set of d_X -variate polynomials of degree $\leq \ell$ on X , where d_X is the dimension of X . The space of piecewise discontinuous polynomial functions on an element boundary is given by

$$\mathbb{P}^\ell(\mathcal{F}_T) := \{v \in L^1(\partial T) : v|_F \in \mathbb{P}^\ell(F) \quad \forall F \in \mathcal{F}_T\}. \quad (2.2)$$

The L^2 orthogonal projector $\pi_X^{0,\ell} : L^1(X) \rightarrow \mathbb{P}^\ell(X)$ is defined as the unique polynomial satisfying

$$(v - \pi_X^{0,\ell} v, w)_X = 0 \quad \forall w \in \mathbb{P}^\ell(X). \quad (2.3)$$

Fix two natural numbers $k, l \in \mathbb{N}$, $l \geq k - 1$. For each element $T \in \mathcal{T}_h$, the local space of unknowns is defined as

$$\underline{U}_T^{k,l} := \mathbb{P}^l(T) \times \mathbb{P}^k(\mathcal{F}_T).$$

We endow the space $\underline{U}_T^{k,l}$ with the discrete energy-like seminorm $\|\cdot\|_{1,T}$ defined for all $\underline{v}_T = (v_T, v_{\partial T}) \in \underline{U}_T^{k,l}$ via

$$\|\underline{v}_T\|_{1,T}^2 := \|\nabla v_T\|_T^2 + h_T^{-1} \|v_{\partial T} - v_T\|_{\partial T}^2. \quad (2.4)$$

On each element we locally reconstruct a potential from the space of unknowns via the operator $p_T^{k+1} : \underline{U}_T^{k,l} \rightarrow \mathbb{P}^{k+1}(T)$ defined to satisfy, for all $\underline{v}_T \in \underline{U}_T^{k,l}$ and $w \in \mathbb{P}^{k+1}(T)$,

$$(\nabla p_T^{k+1} \underline{v}_T, \nabla w)_T = -(v_T, \Delta w)_T + (v_{\partial T}, \nabla w \cdot \mathbf{n}_{\partial T})_{\partial T}, \quad (2.5)$$

$$(v_T - p_T^{k+1} \underline{v}_T, 1)_T = 0. \quad (2.6)$$

This potential reconstruction allows us to approximate $a(u, v)$ on each element by the bilinear form $a_T : \underline{U}_T^{k,l} \times \underline{U}_T^{k,l} \rightarrow \mathbb{R}$ defined as

$$a_T(\underline{u}_T, \underline{v}_T) := (\nabla p_T^{k+1} \underline{u}_T, \nabla p_T^{k+1} \underline{v}_T)_T + s_T(\underline{u}_T, \underline{v}_T), \quad (2.7)$$

where $s_T : \underline{U}_T^{k,l} \times \underline{U}_T^{k,l} \rightarrow \mathbb{R}$ is a symmetric, positive semi-definite stabilisation such that

$$c(l, k)^{-1} \|\underline{v}_T\|_{1,T}^2 \lesssim a_T(\underline{v}_T, \underline{v}_T) \lesssim c(l, k)(k+1)^2 \|\underline{v}_T\|_{1,T}^2. \quad (2.8)$$

where

$$c(l, k) = \begin{cases} (l+1)^2 & \text{if } l \leq k, \\ 1 & \text{if } l \geq k+1. \end{cases} \quad (2.9)$$

We consider throughout this work the gradient-based stabilisation form defined in [20]

$$s_T^\nabla(\underline{u}_T, \underline{v}_T) := (\nabla \delta_T^l \underline{u}_T, \nabla \delta_T^l \underline{v}_T)_T + h_T^{-1} (\delta_{\partial T}^k \underline{u}_T, \delta_{\partial T}^k \underline{v}_T)_{\partial T}, \quad (2.10)$$

where $\delta_T^l : \underline{U}_T^{k,l} \rightarrow \mathbb{P}^l(T)$ and $\delta_{\partial T}^k : \underline{U}_T^{k,l} \rightarrow \mathbb{P}^k(\mathcal{F}_T)$ denote the difference operators defined for all $\underline{v}_T \in \underline{U}_T^{k,l}$ by

$$\delta_T^l \underline{v}_T := \pi_T^{0,l} (p_T^{k+1} \underline{v}_T - v_T) \quad \text{and} \quad \delta_{\partial T}^k \underline{v}_T := \pi_{\partial T}^{0,k} (p_T^{k+1} \underline{v}_T - v_{\partial T}).$$

Here, $\pi_{\partial T}^{0,k}$ is the projector onto the space $\mathbb{P}^k(\mathcal{F}_T)$ satisfying $\pi_{\partial T}^{0,k} v|_F = \pi_F^{0,k} v$ for all $F \in \mathcal{F}_T$ and $v \in L^1(\partial T)$. We show in Section 3.2 that the stabilisation (2.10) satisfies (2.8) (which justifies our choice of $c(l, k)$, although we believe but cannot prove yet that $c(l, k) = 1$ is also a valid choice, see Remark 4).

2.2.2 Global formulation

The global space of unknowns is defined as

$$\underline{U}_h^{k,l} := \left\{ \underline{v}_h = ((v_T)_{T \in \mathcal{T}_h}, (v_F)_{F \in \mathcal{F}_h}) : v_T \in \mathbb{P}^l(T) \quad \forall T \in \mathcal{T}_h, v_F \in \mathbb{P}^k(F) \quad \forall F \in \mathcal{F}_h \right\}.$$

To account for the homogeneous boundary conditions, the following subspace is also introduced:

$$\underline{U}_{h,0}^{k,l} := \{ \underline{v}_h \in \underline{U}_h^{k,l} : v_F = 0 \quad \forall F \in \mathcal{F}_h^b \}.$$

For any $\underline{v}_h \in \underline{U}_h^{k,l}$ we denote its restriction to an element T by $\underline{v}_T = (v_T, v_{\partial T}) \in \underline{U}_T^{k,l}$ (where, naturally, $v_{\partial T}$ is defined from $(v_F)_{F \in \mathcal{F}_T}$). We also denote by v_h the piecewise polynomial function satisfying $v_h|_T = v_T$ for all $T \in \mathcal{T}_h$.

The global bilinear forms $\mathbf{a}_h : \underline{U}_h^{k,l} \times \underline{U}_h^{k,l} \rightarrow \mathbb{R}$ and $\mathbf{s}_h : \underline{U}_h^{k,l} \times \underline{U}_h^{k,l} \rightarrow \mathbb{R}$ are defined as

$$\mathbf{a}_h(\underline{u}_h, \underline{v}_h) := \sum_{T \in \mathcal{T}_h} \mathbf{a}_T(\underline{u}_T, \underline{v}_T) \quad \text{and} \quad \mathbf{s}_h(\underline{u}_h, \underline{v}_h) := \sum_{T \in \mathcal{T}_h} \mathbf{s}_T(\underline{u}_T, \underline{v}_T).$$

We also define the discrete energy norm $\|\cdot\|_{\mathbf{a},h}$ on $\underline{U}_{h,0}^{k,l}$ as

$$\|\underline{v}_h\|_{\mathbf{a},h} := \mathbf{a}_h(\underline{v}_h, \underline{v}_h)^{\frac{1}{2}} \quad \forall \underline{v}_h \in \underline{U}_{h,0}^{k,l}. \quad (2.11)$$

The HHO scheme reads: find $\underline{u}_h \in \underline{U}_{h,0}^{k,l}$ such that

$$\mathbf{a}_h(\underline{u}_h, \underline{v}_h) = \mathcal{L}_h(v_h) \quad \forall \underline{v}_h \in \underline{U}_{h,0}^{k,l}, \quad (2.12)$$

where $\mathcal{L}_h : \underline{U}_{h,0}^{k,l} \rightarrow \mathbb{R}$ is a linear form defined as

$$\mathcal{L}_h(v_h) := \sum_{T \in \mathcal{T}_h} (f, v_T)_T.$$

2.2.3 Statically condensed system and eigenvalue estimates

The static condensation procedure, as outlined in [15, Appendix B.3], allows the elimination of the element unknowns. Selecting \underline{v}_h with one free element component v_T , and all other element and face components vanishing, we see that the solution \underline{u}_h to problem (2.12) satisfies for all $T \in \mathcal{T}_h$ and $v_T \in \mathbb{P}^l(T)$

$$\mathbf{a}_T((u_T, u_{\partial T}), (v_T, 0)) = (f, v_T)_T.$$

This can be alternatively written as

$$\mathbf{a}_T((u_T, 0), (v_T, 0)) = (f, v_T)_T - \mathbf{a}_T((0, u_{\partial T}), (v_T, 0)).$$

Noting that the bilinear form $(u_T, v_T) \in \mathbb{P}^k(T) \times \mathbb{P}^k(T) \mapsto \mathbf{a}_T((u_T, 0), (v_T, 0))$ is coercive (due to (2.8)), we can define the polynomial $g_T \in \mathbb{P}^l(T)$ and the linear operator $\mathcal{S}_T : \mathbb{P}^k(\mathcal{F}_T) \rightarrow \mathbb{P}^l(T)$ via

$$\mathbf{a}_T((g_T, 0), (v_T, 0)) = (f, v_T)_T \quad \forall v_T \in \mathbb{P}^l(T), \quad (2.13)$$

$$\mathbf{a}_T((\mathcal{S}_T u_{\partial T}, 0), (v_T, 0)) = -\mathbf{a}_T((0, u_{\partial T}), (v_T, 0)) \quad \forall v_T \in \mathbb{P}^l(T). \quad (2.14)$$

Therefore, u_T is calculated from $u_{\partial T}$ via the affine transformation

$$u_T = \mathcal{S}_T u_{\partial T} + g_T. \quad (2.15)$$

Substituting (2.15) into (2.12) and testing against $\underline{v}_h = (0, v_{\mathcal{F}_h}) = ((0)_{T \in \mathcal{T}_h}, (v_F)_{F \in \mathcal{F}_h}) \in \underline{U}_{h,0}^{k,l}$ yields

$$\sum_{T \in \mathcal{T}_h} a_T((\mathcal{S}_T u_{\partial T}, u_{\partial T}), (0, v_{\partial T})) + \sum_{T \in \mathcal{T}_h} a_T((g_T, 0), (0, v_{\partial T})) = 0.$$

Setting

$$\mathbb{P}_0^k(\mathcal{F}_h) := \{u_{\mathcal{F}_h} = (u_F)_{F \in \mathcal{F}_h} : u_F \in \mathbb{P}^k(F) \quad \forall F \in \mathcal{F}_h, \quad u_F = 0 \text{ if } F \subset \partial\Omega\},$$

the statically condensed problem then reads: Find $u_{\mathcal{F}_h} \in \mathbb{P}_0^k(\mathcal{F}_h)$ such that

$$\mathbf{A}_h(u_{\mathcal{F}_h}, v_{\mathcal{F}_h}) = \mathbf{L}_h(v_{\mathcal{F}_h}) \quad \forall v_{\mathcal{F}_h} \in \mathbb{P}_0^k(\mathcal{F}_h), \quad (2.16)$$

where

$$\begin{aligned} \mathbf{A}_h(u_{\mathcal{F}_h}, v_{\mathcal{F}_h}) &:= \sum_{T \in \mathcal{T}_h} a_T((\mathcal{S}_T u_{\partial T}, u_{\partial T}), (0, v_{\partial T})), \\ \mathbf{L}_h(v_{\mathcal{F}_h}) &:= \sum_{T \in \mathcal{T}_h} -a_T((g_T, 0), (0, v_{\partial T})). \end{aligned}$$

Upon choosing bases of the spaces $\mathbb{P}^k(F)$ for $F \in \mathcal{F}_h^i$, (2.16) takes the equivalent algebraic form

$$\mathbf{A}_h \mathbf{U} = \mathbf{F}$$

where \mathbf{A}_h is the matrix of the bilinear form \mathbf{A}_h , \mathbf{U} the vector of unknowns and \mathbf{F} the source term corresponding to \mathbf{L}_h . Our main result is the following; its proof is given in Section 3.1.

Theorem 1 (Eigenvalue and condition number estimates). *For each $F \in \mathcal{F}_h^i$, denote by T_F^+, T_F^- the two elements on each side of F , and define the characteristic lengths $H_{\mathcal{F}_h, \min}$ and $H_{\mathcal{F}_h, \max}$ by*

$$H_{\mathcal{F}_h, \min} = \min_{F \in \mathcal{F}_h} (h_{T_F^+} + h_{T_F^-}), \quad H_{\mathcal{F}_h, \max}^{-1} = \max_{F \in \mathcal{F}_h} (h_{T_F^+}^{-1} + h_{T_F^-}^{-1}).$$

If, for each $F \in \mathcal{F}_h^i$, the basis on $\mathbb{P}^k(F)$ is orthonormal for the $L^2(F)$ -inner product, then the minimal eigenvalue, maximal eigenvalue and condition number of \mathbf{A}_h satisfy

$$\lambda_{\min}(\mathbf{A}_h) \gtrsim c(l, k)^{-1} H_{\mathcal{F}_h, \min}, \quad (2.17a)$$

$$\lambda_{\max}(\mathbf{A}_h) \lesssim c(l, k)(k+1)^2 H_{\mathcal{F}_h, \max}^{-1}, \quad (2.17b)$$

$$\kappa(\mathbf{A}_h) \lesssim c(l, k)^2 (k+1)^2 H_{\mathcal{F}_h, \max}^{-1} H_{\mathcal{F}_h, \min}. \quad (2.17c)$$

Remark 1 (Characteristic lengths). *Setting $h_{\min} = \min_{T \in \mathcal{T}_h} h_T$, we have $H_{\mathcal{F}_h, \min} \gtrsim h_{\min}$ and $H_{\mathcal{F}_h, \max}^{-1} \lesssim h_{\min}^{-1}$. Hence, (2.17) leads to the bounds*

$$\lambda_{\min}(\mathbf{A}_h) \gtrsim c(l, k)^{-1} h_{\min}, \quad \lambda_{\max}(\mathbf{A}_h) \lesssim c(l, k)(k+1)^2 h_{\min}^{-1}, \quad \kappa(\mathbf{A}_h) \lesssim c(l, k)^2 (k+1)^2 h_{\min}^{-2}.$$

For quasi-uniform meshes, h_{\min} can be replaced above by h in these estimates. However, on specific meshes (especially cut meshes with small cut elements), (2.17) can lead to much better estimates than those purely based on h_{\min} ; see Section 5.

Remark 2 (Small faces). *The estimates (2.17) are totally independent of the maximum number of faces in each element, or on their diameter, and are therefore fully robust with respect to small faces.*

Remark 3 (Coefficient $c(l, k)$). *We conjecture that the gradient-based stabilisation actually satisfies (2.8) with $c(l, k) = 1$, see Remark 4. If that is the case, then all $c(l, k)$ above can be removed and we recover the more expected dependency in $\mathcal{O}((k+1)^2)$ of the condition number with respect to the method's order.*

3 Proofs

3.1 Estimate on the eigenvalues

Let us start with two preliminary estimates. The proof of the following trace inequality can be found in [11, Section 3].

Lemma 2 (Trace Inequality). *For all $v \in H^1(T)$,*

$$\|v\|_{\partial T}^2 \lesssim h_T^{-1} \left(\|v\|_T^2 + h_T^2 \|\nabla v\|_T^2 \right). \quad (3.1)$$

For $v \in \mathbb{P}^\ell(T)$, the following discrete trace inequality also holds:

$$\|v\|_{\partial T}^2 \lesssim h_T^{-1} (\ell + 1)(\ell + d) \|v\|_T^2. \quad (3.2)$$

The proof of the discrete Poincaré inequality follows a similar procedure to [15, Lemma 2.15], however we provide it here robust with respect to small faces and polynomial degrees k, l .

Lemma 3 (Discrete Poincaré inequality). *For all $\underline{v}_h \in \underline{U}_{h,0}^{k,l}$ it holds that*

$$\|v_h\|_\Omega \lesssim c(l, k)^{\frac{1}{2}} \|\underline{v}_h\|_{a,h}. \quad (3.3)$$

Proof. As the divergence operator $\nabla \cdot : H^1(\Omega)^d \rightarrow L^2(\Omega)$ is onto, there exists a $\boldsymbol{\tau} \in H^1(\Omega)^d$ such that $\nabla \cdot \boldsymbol{\tau} = v_h$ and $\|\boldsymbol{\tau}\|_{H^1(\Omega)^d} \lesssim \|v_h\|_\Omega$ for every $T \in \mathcal{T}_h$ [15, Lemma 8.3]. Therefore

$$\|v_T\|_T^2 = (v_T, \nabla \cdot \boldsymbol{\tau})_T = -(\nabla v_T, \boldsymbol{\tau})_T + (v_T, \boldsymbol{\tau} \cdot \mathbf{n}_{\partial T})_{\partial T}. \quad (3.4)$$

By the homogeneous condition on the discrete space it holds that

$$\sum_{T \in \mathcal{T}_h} (v_{\partial T}, \boldsymbol{\tau} \cdot \mathbf{n}_{\partial T})_{\partial T} = 0. \quad (3.5)$$

Thus, combining (3.4) and (3.5) and applying a continuous Cauchy–Schwarz inequality followed by a discrete Cauchy–Schwarz inequality on the sum,

$$\begin{aligned} \|v_h\|_\Omega^2 &= - \sum_{T \in \mathcal{T}_h} \left((\nabla v_T, \boldsymbol{\tau})_T + (v_{\partial T} - v_T, \boldsymbol{\tau} \cdot \mathbf{n}_{\partial T})_{\partial T} \right) \\ &\leq \sum_{T \in \mathcal{T}_h} \left(\|\nabla v_T\|_T \|\boldsymbol{\tau}\|_T + \|v_{\partial T} - v_T\|_{\partial T} \|\boldsymbol{\tau}\|_{\partial T} \right) \\ &\leq \sum_{T \in \mathcal{T}_h} \left(\|\nabla v_T\|_T + h_T^{-\frac{1}{2}} \|v_{\partial T} - v_T\|_{\partial T} \right) \left(\|\boldsymbol{\tau}\|_T + h_T^{\frac{1}{2}} \|\boldsymbol{\tau}\|_{\partial T} \right) \\ &\lesssim \left(\sum_{T \in \mathcal{T}_h} \|\underline{v}_T\|_{1,T}^2 \right)^{\frac{1}{2}} \left(\sum_{T \in \mathcal{T}_h} (\|\boldsymbol{\tau}\|_T + h_T^{\frac{1}{2}} \|\boldsymbol{\tau}\|_{\partial T})^2 \right)^{\frac{1}{2}}. \end{aligned}$$

By the coercivity condition (2.8) it holds that

$$c(l, k)^{-\frac{1}{2}} \left(\sum_{T \in \mathcal{T}_h} \|\underline{v}_T\|_{1,T}^2 \right)^{\frac{1}{2}} \lesssim \|\underline{v}_h\|_{a,h}.$$

Invoking a continuous trace inequality (3.1), the bound $h_T \leq h_\Omega$, and the assumption on $\boldsymbol{\tau}$ we infer that

$$\left(\sum_{T \in \mathcal{T}_h} (\|\boldsymbol{\tau}\|_T + h_T^{\frac{1}{2}} \|\boldsymbol{\tau}\|_{\partial T})^2 \right)^{\frac{1}{2}} \lesssim \|\boldsymbol{\tau}\|_{H^1(\Omega)^d} \lesssim \|v_h\|_\Omega.$$

Therefore, $\|v_h\|_\Omega^2 \lesssim c(l, k)^{\frac{1}{2}} \|v_h\|_\Omega \|\underline{v}_h\|_{a,h}$ and simplifying by $\|v_h\|_\Omega$ completes the proof. \square

Corollary 4. For all $\underline{v}_h \in \underline{U}_{h,0}^{k,l}$, it holds that

$$\sum_{T \in \mathcal{T}_h} h_T \|v_{\partial T}\|_{\partial T}^2 \lesssim c(l, k) \|\underline{v}_h\|_{a,h}^2. \quad (3.6)$$

Proof. Consider by a triangle inequality and a continuous trace inequality (3.1),

$$\begin{aligned} \sum_{T \in \mathcal{T}_h} h_T \|v_{\partial T}\|_{\partial T}^2 &\lesssim \sum_{T \in \mathcal{T}_h} \left(h_T \|v_{\partial T} - v_T\|_{\partial T}^2 + \|v_T\|_T^2 + h_T^2 \|\nabla v_T\|_T^2 \right) \\ &= \sum_{T \in \mathcal{T}_h} \left(h_T^2 \|\underline{v}_T\|_{1,T}^2 + \|v_T\|_T^2 \right). \end{aligned}$$

The proof then follows from (2.8) and (3.3). \square

We can now prove the estimates (2.17) on the eigenvalues and condition number of \mathbf{A}_h .

Proof of Theorem 1. We note, from equation (2.14), that for all $v_T \in \mathbb{P}^l(T)$

$$a_T((\mathcal{S}_T u_{\partial T}, u_{\partial T}), (v_T, 0)) = 0.$$

Therefore, setting $v_T = \mathcal{S}_T u_{\partial T}$ and adding to $a_T((\mathcal{S}_T u_{\partial T}, u_{\partial T}), (0, u_{\partial T}))$,

$$a_T((\mathcal{S}_T u_{\partial T}, u_{\partial T}), (0, u_{\partial T})) = a_T((\mathcal{S}_T u_{\partial T}, u_{\partial T}), (\mathcal{S}_T u_{\partial T}, u_{\partial T})).$$

By equation (3.6) it thus holds that

$$\sum_{T \in \mathcal{T}_h} h_T \|u_{\partial T}\|_{\partial T}^2 \lesssim c(l, k) \mathbf{A}_h(u_{\mathcal{F}_h}, u_{\mathcal{F}_h}). \quad (3.7)$$

Consider also

$$\begin{aligned} a_T((\mathcal{S}_T u_{\partial T}, u_{\partial T}), (0, u_{\partial T})) &= a_T((0, u_{\partial T}), (0, u_{\partial T})) + a_T((\mathcal{S}_T u_{\partial T}, 0), (0, u_{\partial T})) \\ &= a_T((0, u_{\partial T}), (0, u_{\partial T})) - a_T((\mathcal{S}_T u_{\partial T}, 0), (\mathcal{S}_T u_{\partial T}, 0)), \\ &\leq a_T((0, u_{\partial T}), (0, u_{\partial T})) \end{aligned}$$

where the second line follows from equation (2.14) and the symmetry of a_T , and the conclusion from the fact that a_T is semi-definite positive. Therefore, by the boundedness (2.8) of a_T ,

$$a_T((\mathcal{S}_T u_{\partial T}, u_{\partial T}), (0, u_{\partial T})) \lesssim c(l, k)(k+1)^2 h_T^{-1} \|u_{\partial T}\|_{\partial T}^2. \quad (3.8)$$

Thus, combining (3.7) and (3.8) it holds that

$$c(l, k)^{-1} \sum_{T \in \mathcal{T}_h} h_T \|u_{\partial T}\|_{\partial T}^2 \lesssim \mathbf{A}_h(u_{\mathcal{F}_h}, u_{\mathcal{F}_h}) \lesssim c(l, k)(k+1)^2 \sum_{T \in \mathcal{T}_h} h_T^{-1} \|u_{\partial T}\|_{\partial T}^2.$$

Gathering by faces (and recalling that $u_{\mathcal{F}_h}$ vanishes on boundary faces), we obtain

$$c(l, k)^{-1} \sum_{F \in \mathcal{F}_h^i} (h_{T_F^+} + h_{T_F^-}) \|u_F\|_F^2 \lesssim \mathbf{A}_h(u_{\mathcal{F}_h}, u_{\mathcal{F}_h}) \lesssim c(l, k)(k+1)^2 \sum_{F \in \mathcal{F}_h^i} (h_{T_F^+}^{-1} + h_{T_F^-}^{-1}) \|u_F\|_F^2.$$

Having chosen orthonormal bases on the space $\mathbb{P}^k(F)$, and recalling the definitions of $H_{\mathcal{F}_h, \min}$ and $H_{\mathcal{F}_h, \max}$, this relation boils down to

$$c(l, k)^{-1} H_{\mathcal{F}_h, \min} \mathbf{U} \cdot \mathbf{U} \lesssim \mathbf{A}_h \mathbf{U} \cdot \mathbf{U} \lesssim c(l, k)(k+1)^2 H_{\mathcal{F}_h, \max}^{-1} \mathbf{U} \cdot \mathbf{U}.$$

The estimates (2.17) follow trivially. \square

3.2 Analysis of the gradient-based stabilisation

We prove here that the stabilisation s_T^∇ defined by (2.10) satisfies the coercivity and boundedness assumption (2.8). We start with preliminary estimates.

Lemma 5 (Poincaré–Wirtinger). *For all $v \in H^1(T)$ the following Poincaré–Wirtinger inequality holds:*

$$\|v - \pi_T^{0,0} v\|_T \lesssim h_T |v|_{H^1(T)}. \quad (3.9)$$

Proof. See [15, Remark 1.46]. \square

Lemma 6 (Approximation properties of $\pi_{\partial T}^{0,\ell}$). *For all $v \in H^1(T)$ and $\ell \geq 0$, it holds that*

$$h_T^{-1} \|v - \pi_{\partial T}^{0,\ell} v\|_{\partial T}^2 \lesssim |v|_{H^1(T)}^2 \quad (3.10)$$

Proof. As orthogonal projectors minimise their respective norms, and $\mathbb{P}^0(T)|_{\partial T} \subset \mathbb{P}^\ell(\partial T)$ we may replace $\pi_{\partial T}^{0,\ell}$ with $\pi_T^{0,0}$ in the boundary norm and invoke a continuous trace inequality (3.1) to see that

$$\|v - \pi_{\partial T}^{0,\ell} v\|_{\partial T} \leq \|v - \pi_T^{0,0} v\|_{\partial T} \lesssim h_T^{-\frac{1}{2}} \|v - \pi_T^{0,0} v\|_T + h_T^{\frac{1}{2}} |v - \pi_T^{0,0} v|_{H^1(T)} \lesssim h_T^{\frac{1}{2}} |v|_{H^1(T)},$$

where the conclusion follows from a Poincaré–Wirtinger inequality (3.9). \square

Lemma 7 (H^1 -boundedness of $\pi_T^{0,l}$ on $\mathbb{P}^{k+1}(T)$). *For all $v \in \mathbb{P}^{k+1}(T)$,*

$$|\pi_T^{0,l} v|_{H^1(T)}^2 \lesssim c(l, k) |v|_{H^1(T)}^2. \quad (3.11)$$

Remark 4 (About $c(l, k)$). *The constant $c(l, k)$ appears in the estimates of Theorem 1 only because of the estimate above. We conjecture, and this is backed up by numerical tests, that (3.11) actually holds with constant $c(l, k) = 1$, but we are yet unable to prove this.*

Proof. As the dependence (or lack thereof) of the hidden constant on the element diameter is well known (c.f. [15, Remark 1.47]) we shall assume that $h_T = 1$. The estimate is trivial if $l \geq k + 1$ since $\pi_T^{0,l} v = v$ in that case. For the estimate with $l \leq k$ we begin with the triangle inequality

$$|\pi_T^{0,l} v|_{H^1(T)}^2 \lesssim |\pi_T^{0,l} v - v|_{H^1(T)}^2 + |v|_{H^1(T)}^2.$$

Consider the following inverse estimate (see [10, Lemma 4.23])

$$|v - \pi_T^{0,l} v|_{H^1(T)}^2 \lesssim (k + 1)^4 \|v - \pi_T^{0,l} v\|_T^2. \quad (3.12)$$

Due to orthogonal projectors minimising their respective norms, it holds that

$$\|v - \pi_T^{0,l} v\|_T^2 = \min_{q \in \mathbb{P}^l(T)} \|v - q\|_T^2 \lesssim (l + 1)^{-2} \|v\|_{H^1(T)}^2, \quad (3.13)$$

the last inequality following from [1, Appendix A]. Noting that we can replace v by $v - \pi_T^{0,0} v$ without effecting the left hand side of (3.13), we can apply a Poincaré–Wirtinger inequality (3.9) to replace the H^1 -norm with the H^1 -seminorm. Thus, combining with (3.12), we conclude that

$$|v - \pi_T^{0,l} v|_{H^1(T)}^2 \lesssim (k + 1)^4 (l + 1)^{-2} |v|_{H^1(T)}^2 \lesssim (l + 1)^2 |v|_{H^1(T)}^2.$$

\square

Lemma 8 (Coercivity). *The stabilisation term s_T^∇ satisfies for all $\underline{v}_T \in \underline{U}_T^{k,l}$*

$$\|\underline{v}_T\|_{1,T}^2 \lesssim c(l,k) a_T(\underline{v}_T, \underline{v}_T).$$

Proof. Consider by a triangle inequality and the definition (2.7) of a_T

$$\|\nabla v_T\|_T^2 \lesssim \|\nabla(v_T - p_T^{k+1} \underline{v}_T)\|_T^2 + \|\nabla p_T^{k+1} \underline{v}_T\|_T^2 \leq \|\nabla(v_T - p_T^{k+1} \underline{v}_T)\|_T^2 + a_T(\underline{v}_T, \underline{v}_T).$$

Conversely, by applying a triangle inequality on the boundary term of (2.4),

$$\begin{aligned} h_T^{-1} \|v_{\partial T} - v_T\|_{\partial T}^2 &\lesssim h_T^{-1} \|v_{\partial T} - p_T^{k+1} \underline{v}_T\|_{\partial T}^2 + h_T^{-1} \|p_T^{k+1} \underline{v}_T - v_T\|_{\partial T}^2 \\ &\lesssim h_T^{-1} \|v_{\partial T} - p_T^{k+1} \underline{v}_T\|_{\partial T}^2 + \|\nabla(v_T - p_T^{k+1} \underline{v}_T)\|_T^2 \end{aligned}$$

where the conclusion follows from a continuous trace inequality (3.1) and a Poincaré–Wirtinger inequality (3.9). Thus, it remains to show that

$$\|\nabla(v_T - p_T^{k+1} \underline{v}_T)\|_T^2 + h_T^{-1} \|v_{\partial T} - p_T^{k+1} \underline{v}_T\|_{\partial T}^2 \lesssim c(l,k) a_T(\underline{v}_T, \underline{v}_T). \quad (3.14)$$

Consider, by a triangle inequality and the definition (2.10) of s_T^∇ ,

$$\begin{aligned} \|\nabla(v_T - p_T^{k+1} \underline{v}_T)\|_T^2 + h_T^{-1} \|v_{\partial T} - p_T^{k+1} \underline{v}_T\|_{\partial T}^2 \\ = \|\nabla(\delta_T^l \underline{v}_T + (\mathcal{I} - \pi_T^{0,l}) p_T^{k+1} \underline{v}_T)\|_T^2 + h_T^{-1} \|\delta_{\partial T}^k \underline{v}_T + (\mathcal{I} - \pi_{\partial T}^{0,k}) p_T^{k+1} \underline{v}_T\|_{\partial T}^2 \\ \lesssim s_T^\nabla(\underline{v}_T, \underline{v}_T) + \|\nabla(\mathcal{I} - \pi_T^{0,l}) p_T^{k+1} \underline{v}_T\|_T^2 + h_T^{-1} \|(\mathcal{I} - \pi_{\partial T}^{0,k}) p_T^{k+1} \underline{v}_T\|_{\partial T}^2, \end{aligned}$$

where \mathcal{I} denotes the identity operator. It follows from the H^1 -boundedness property (3.11) of $\pi_T^{0,l}$ and the approximation property (3.10) of $\pi_{\partial T}^{0,k}$ that

$$\|\nabla(\mathcal{I} - \pi_T^{0,l}) p_T^{k+1} \underline{v}_T\|_T^2 + h_T^{-1} \|(\mathcal{I} - \pi_{\partial T}^{0,k}) p_T^{k+1} \underline{v}_T\|_{\partial T}^2 \lesssim c(l,k) \|\nabla p_T^{k+1} \underline{v}_T\|_T^2$$

which completes the proof. \square

Lemma 9 (Boundedness). *The stabilisation term s_T^∇ satisfies for all $\underline{v}_T \in \underline{U}_T^{k,l}$*

$$a_T(\underline{v}_T, \underline{v}_T) \lesssim c(l,k)(k+1)^2 \|\underline{v}_T\|_{1,T}^2. \quad (3.15)$$

Proof. Consider, by the definition (2.5) of p_T^{k+1} , an integration-by-parts and a discrete trace inequality (3.2) noting that $\nabla p_T^{k+1} \underline{v}_T \in \mathbb{P}^k(T)^d$,

$$\begin{aligned} \|\nabla p_T^{k+1} \underline{v}_T\|_T^2 &= (\nabla v_T, \nabla p_T^{k+1} \underline{v}_T)_T + (v_{\partial T} - v_T, \nabla p_T^{k+1} \underline{v}_T \cdot \mathbf{n}_{\partial T})_{\partial T} \\ &\leq \|\nabla v_T\|_T \|\nabla p_T^{k+1} \underline{v}_T\|_T + \|v_{\partial T} - v_T\|_{\partial T} \|\nabla p_T^{k+1} \underline{v}_T\|_{\partial T} \\ &\lesssim \|\nabla p_T^{k+1} \underline{v}_T\|_T \left(\|\nabla v_T\|_T + (h_T^{-1}(k+1)(k+d))^{\frac{1}{2}} \|v_{\partial T} - v_T\|_{\partial T} \right). \end{aligned}$$

Simplifying by $\|\nabla p_T^{k+1} \underline{v}_T\|_T$ and squaring we conclude that

$$\|\nabla p_T^{k+1} \underline{v}_T\|_T^2 \lesssim (k+1)^2 \|\underline{v}_T\|_{1,T}^2. \quad (3.16)$$

We turn now to bounding the stabilisation term. It follows from a triangle inequality and the boundedness properties of $\pi_T^{0,l}$ (see (3.11)) and $\pi_{\partial T}^{0,k}$ (which is $L^2(\partial T)$ -bounded by construction) that

$$s_T^\nabla(\underline{v}_T, \underline{v}_T) \lesssim c(l,k) \|\nabla(v_T - p_T^{k+1} \underline{v}_T)\|_T^2 + h_T^{-1} \|v_{\partial T} - p_T^{k+1} \underline{v}_T\|_{\partial T}^2. \quad (3.17)$$

By a triangle inequality, a continuous trace inequality (3.1), and a Poincaré–Wirtinger inequality (3.9) due to the zero mean value of $v_T - \mathbf{p}_T^{k+1} \underline{v}_T$ (see (2.6)) it holds that

$$h_T^{-1} \|v_{\partial T} - \mathbf{p}_T^{k+1} \underline{v}_T\|_{\partial T}^2 \lesssim h_T^{-1} \|v_{\partial T} - v_T\|_{\partial T}^2 + \|\nabla(v_T - \mathbf{p}_T^{k+1} \underline{v}_T)\|_T^2. \quad (3.18)$$

Thus, combining (3.17) and (3.18), and applying a triangle inequality we conclude that

$$s_T^\nabla(\underline{v}_T, \underline{v}_T) \lesssim c(l, k) \left(\|\underline{v}_T\|_{1,T}^2 + \|\nabla \mathbf{p}_T^{k+1} \underline{v}_T\|_T^2 \right)$$

and the proof follows from (3.16). \square

4 HHO on unfitted meshes

As discussed in the introduction, the generation of unstructured body-fitted meshes of geometrically complex regions – such as those with curved boundaries and high curvatures – can present great difficulties. Unfitted finite element methods avoid this issue because they are defined on a simple (e.g., Cartesian or octree) background mesh covering the domain of interest. The elements in touch with interface boundaries can be locally cut to produce polytopal elements on the physical domain boundaries. These cuts can produce narrow, anisotropic ‘sliver-cut’ elements, as well as small but round ‘small-cut’ elements.

The design of a variant of the HHO method on unfitted meshes, with potentially curved elements, is presented and analysed in [8] for elliptic interface problems. The unfitted HHO method therein makes use of Nitsche’s method for the local reconstruction operator. Instead, we consider a standard HHO method on unfitted meshes. In particular, we define a simple structured background mesh $\mathcal{T}_h^{\text{bg}}$ and extract the submesh of active elements $\mathcal{T}_h^{\text{act}}$. The active mesh is split into interior elements $\mathcal{T}_h^{\text{in}}$ and cut elements $\mathcal{T}_h^{\text{cut}}$.

Based on the condition number bounds in Theorem 1, we know that the conditioning of the system matrix can be severely affected by the presence of small-cut and sliver-cut elements. To attain bounded condition number on cut meshes that are independent of the cut location, sliver-cut and small-cut elements in $\mathcal{T}_h^{\text{cut}}$ are aggregated to their neighbours to form an isotropic, quasi-uniform mesh. In particular, we iterate over elements $T \in \mathcal{T}_h^{\text{cut}}$ and merge T with its neighbour sharing the longest edge (or face) if

$$\frac{|T|_d}{|\partial T|_{d-1}} < \epsilon_1 h_T \quad \text{or} \quad h_T < \epsilon_2 h_{\max}.$$

The algorithm is re-run till no ill-posed elements are found. We take $\epsilon_1 = 0.05$ and $\epsilon_2 = 0.3$ in the numerical experiments section. After this aggregation step, we end up with a new mesh $\mathcal{T}_h^{\text{ag}}$. Let us note that arbitrarily small faces can still be present in $\mathcal{T}_h^{\text{ag}}$. The following corollary is a direct consequence of Theorem 1 and the aggregation algorithm.

Corollary 10 (Eigenvalues and condition numbers on unfitted meshes). *Let $\mathcal{T}_h^{\text{bg}}$ be a background mesh covering Ω with characteristic mesh size h and $\mathcal{T}_h^{\text{ag}}$ the corresponding aggregated mesh obtained using the algorithm described above. Let \mathbf{A}_h be the linear system matrix corresponding to the HHO discretisation (2.16) for $\mathcal{T}_h^{\text{ag}}$. Under the assumptions in Theorem 1, it holds:*

$$\lambda_{\min}(\mathbf{A}_h) \gtrsim c(l, k)^{-1} h, \quad \lambda_{\max}(\mathbf{A}_h) \lesssim c(l, k)(k+1)^2 h^{-1}, \quad \kappa(\mathbf{A}_h) \lesssim c(l, k)^2 (k+1)^2 h^{-2},$$

where the constants are independent of the cut location but depend on the choice of ϵ_1 and ϵ_2 .

We note that the ill-conditioning of systems arising in unfitted \mathcal{C}^0 Lagrangian FEs can be solved by aggregating ill-conditioned elements into their neighbours [4]. However, the strategy we consider here is simpler because there is no need to eliminate ill-posed nodes via constraints in each aggregate.

5 Numerical Results

We provide here a numerical analysis of the condition number to illustrate the results derived in previous sections. The linear system (2.16) is assembled using the **HArDCore** open source C++ library [18]. We compute the condition number using the **SymEigsSolver** solver found in the **Spectra** library, with documentation available at <https://spectralib.org/doc/index.html>. All numerical tests in this section are performed using element degree $l = k$, and L^2 -orthonormalised basis functions.

5.1 Coarsened meshes

In order to capture intricate geometric details in a given domain it is sometimes sensible to start with a regular, fine mesh of small element diameter, and agglomerate elements together in order to save computation time. These coarsened meshes are (relatively) isotropic and quasi-uniform, however can have many faces per element and arbitrarily small face diameters. Thus, Theorem 1 predicts the maximum and minimum eigenvalues to scale as $\lambda_{\min}(\mathbf{A}_h) \approx h$ and $\lambda_{\max}(\mathbf{A}_h) \approx h^{-1}$ respectively, independently of the number and size of faces in each element. We consider the unit box $\Omega = (0, 1)^2 \subset \mathbb{R}^2$, and a fine triangular mesh of Ω . We then design successive coarsenings of these meshes and observe how the condition number evolves. Such meshes are plotted in Figure 1 with the data of the mesh sequence presented in Table 1.

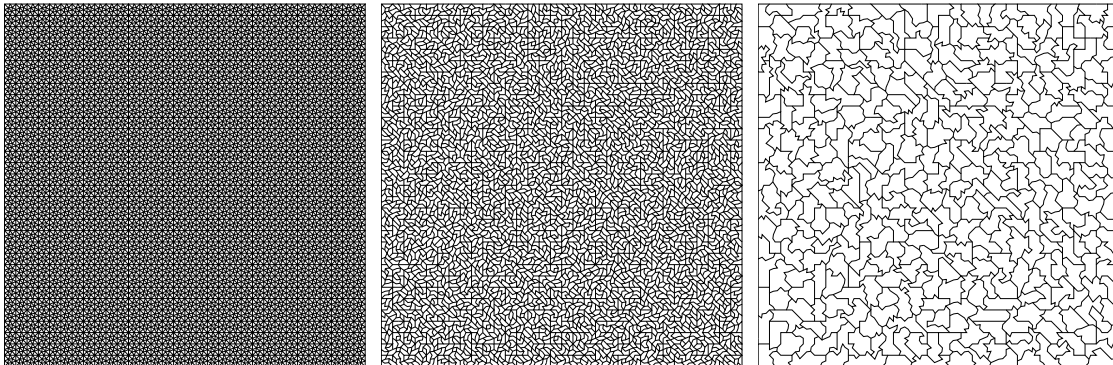


Figure 1: Coarsened meshes

h_{\min}	h_{\max}	Nb. Elements	Nb. Internal Edges
$1.19 \cdot 10^{-2}$	$1.56 \cdot 10^{-2}$	14,336	21,376
$1.19 \cdot 10^{-2}$	$2.38 \cdot 10^{-2}$	8,066	15,106
$1.56 \cdot 10^{-2}$	$3.49 \cdot 10^{-2}$	4,440	11,480
$2.21 \cdot 10^{-2}$	$6.25 \cdot 10^{-2}$	2,390	8,783
$2.87 \cdot 10^{-2}$	$8.47 \cdot 10^{-2}$	1,285	6,510
$3.76 \cdot 10^{-2}$	0.11	684	4,825
$6.11 \cdot 10^{-2}$	0.13	363	3,633
$7.51 \cdot 10^{-2}$	0.19	193	2,708
0.11	0.24	103	2,020
0.14	0.33	56	1,488
0.24	0.49	29	1,056

Table 1: Coarsened meshes

The condition number and eigenvalues on each mesh are plotted in Figure 2. As the mesh is coarsened the condition number appears to decay slightly slower than h^{-2} . This is easily explainable due to the successive meshes becoming less ‘round’, and thus the mesh regularity parameter increasing slightly with each level of coarsening.

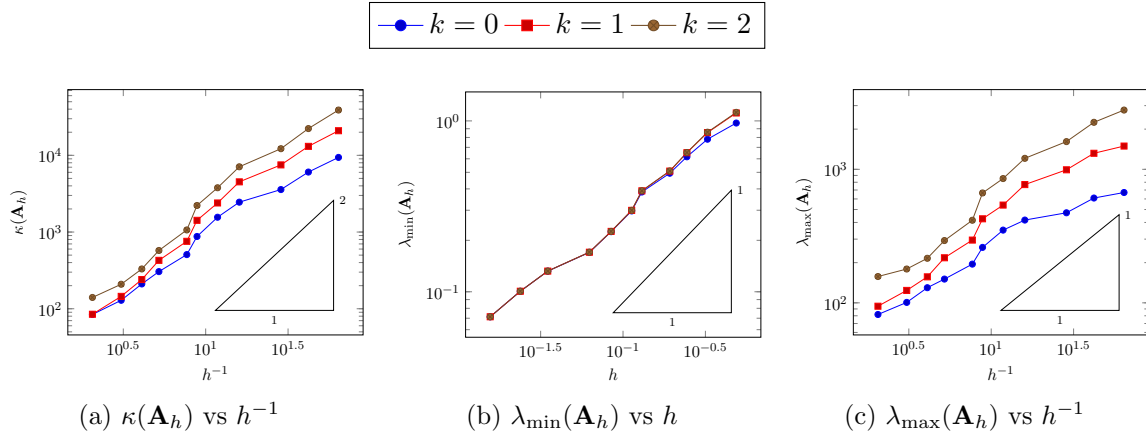


Figure 2: Coarse square meshes

5.2 Unfitted Meshes

In this section, we apply the HHO method to unfitted meshes using the aggregation strategy proposed above. The computation of the unfitted meshes and the boundary-element intersections has been carried out using the **Gridap** open-source Julia library [3] version 0.16.3 and its extension package for unfitted methods **GridapEmbedded.jl** [27] version 0.7. We have considered first-order boundary representations.

5.2.1 Test A

Take the circular domain $\Omega = \{(x, y) \in \mathbb{R}^2 : x^2 + y^2 < 1\} \subset \mathbb{R}^2$ and consider three similar cut meshes of Ω , with a parameter ϵ controlling the diameter of the smallest cut elements ($\epsilon < h_T$ for all $T \in \mathcal{T}_h$). The mesh data is given in Table 2, and we plot values of the condition number and eigenvalues versus ϵ in Figure 3. It is clear that both the maximum eigenvalue, and the condition number become unbounded as $\epsilon \rightarrow 0$. The minimum eigenvalue, however, stays approximately constant. This is consistent with the theory as each face is connected to at least one element with diameter proportional to h_{\max} , thus we expect $\lambda_{\min}(\mathbf{A}_h) \sim h_{\max} = \text{const.}$

ϵ	h_{\min}	h_{\max}	Nb. Elements	Nb. Internal Edges
$1 \cdot 10^{-2}$	$1.14 \cdot 10^{-2}$	0.28	154	202
$1 \cdot 10^{-3}$	$1.13 \cdot 10^{-3}$	0.28	154	202
$1 \cdot 10^{-4}$	$1.13 \cdot 10^{-4}$	0.28	154	202

Table 2: Parameters of the circular meshes with varying values of ϵ

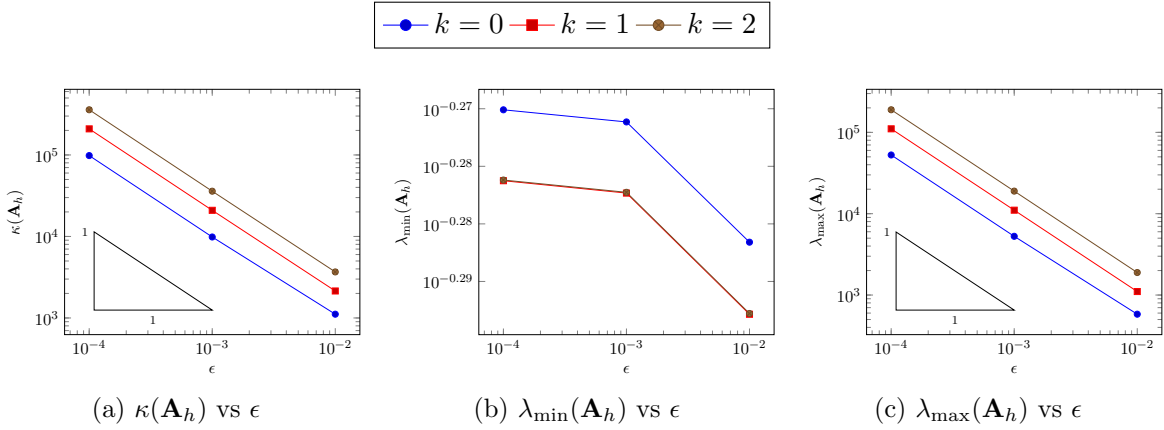


Figure 3: Cut meshes with small-cut elements

To avoid unbounded condition numbers on cut meshes, sliver and small-cut elements are aggregated as explained above. A portion of the resulting aggregated mesh $\mathcal{T}_h^{\text{ag}}$ of Ω is plotted in Figure 4 showing the aggregation of sliver-cut and small-cut elements. We note the existence of arbitrarily small faces after the aggregation of small-cut elements.

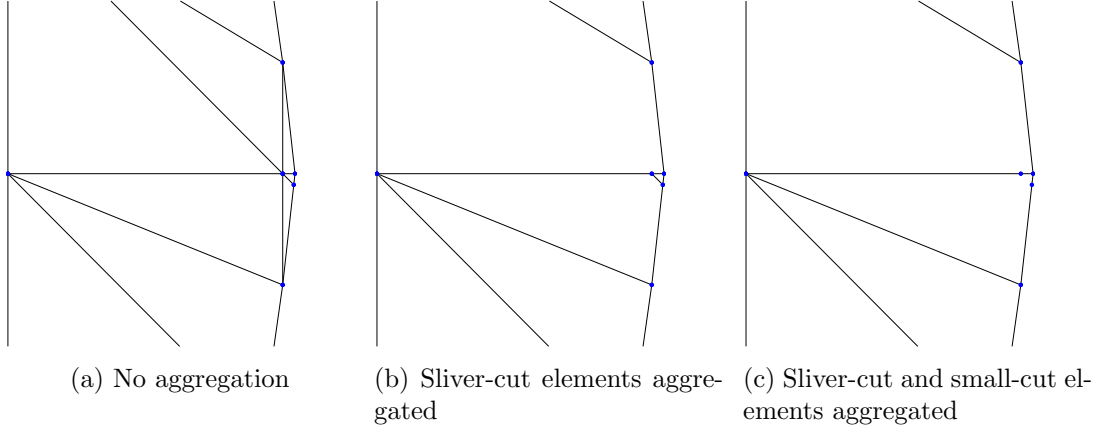


Figure 4: Aggregation of cut meshes

For each mesh in Table 2 we consider a corresponding aggregated mesh, and in Figure 5 we test the condition number and eigenvalues of the system matrix for various polynomial degrees k . It is clear that after aggregation the condition number is independent of ϵ .

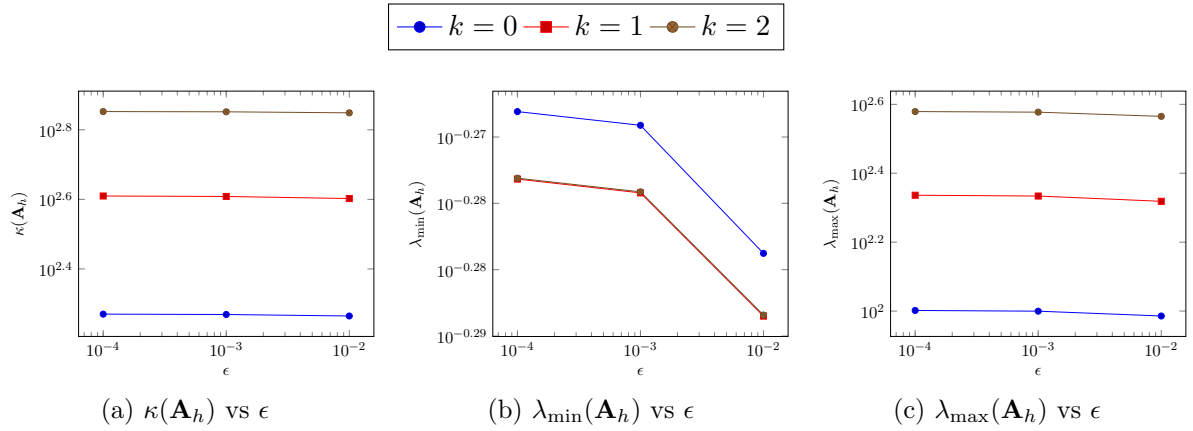


Figure 5: Cut meshes with aggregated elements

5.2.2 Test B

We would now like to consider a sequence of unfitted and approximate meshes of the circular domain $\Omega = \{(x, y) \in \mathbb{R}^2 : x^2 + y^2 < 1\}$ and track the conditioning of the scheme before and after the agglomeration of sliver-cut and small-cut elements. The parameters of this sequence of meshes are given in Table 3 and three of the meshes are plotted in Figure 6.

h_{\min}	h_{\max}	Nb. Elements	Nb. Internal Edges
0.16	0.57	48	59
$1.14 \cdot 10^{-2}$	0.28	154	202
$4.07 \cdot 10^{-3}$	0.14	538	750
$4.7 \cdot 10^{-3}$	$9.43 \cdot 10^{-2}$	1,098	1,562
$2.32 \cdot 10^{-3}$	$7.07 \cdot 10^{-2}$	1,878	2,706

Table 3: Parameters of the meshes used in Test B prior to aggregation

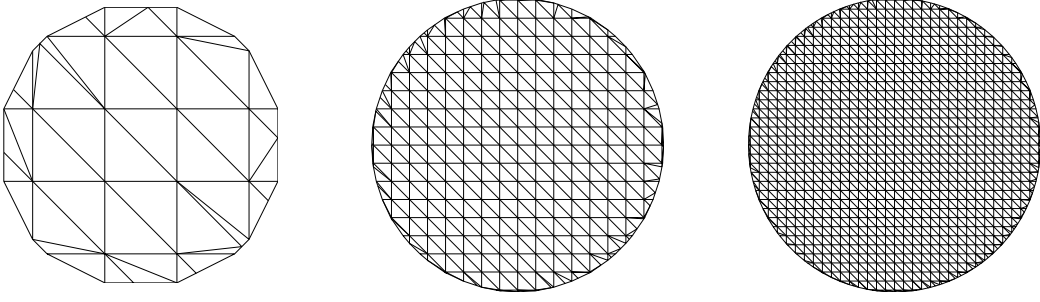


Figure 6: Three of the meshes used in Test B prior to aggregation

Prior to the aggregation of small-cut elements, each face is attached to at least one element of diameter proportional to h_{\max} . Thus we expect to observe $\lambda_{\min}(\mathbf{A}_h) \sim h_{\max}$ and $\lambda_{\max}(\mathbf{A}_h) \sim h_{\min}^{-1}$. In Figure 7 we plot the condition number and eigenvalues for each mesh prior to aggregation. The results are not smooth due to the presence of sliver-cut elements which have potentially very large mesh regularity parameters. In Figure 8, we observe that after the agglomeration of sliver-cut elements the results behave as predicted by theory.

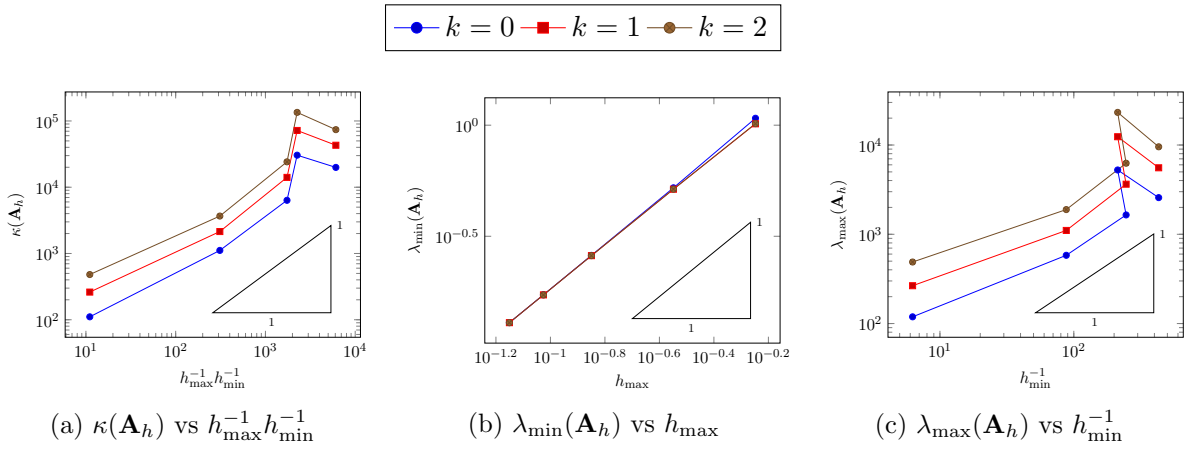


Figure 7: Circular meshes with no aggregation

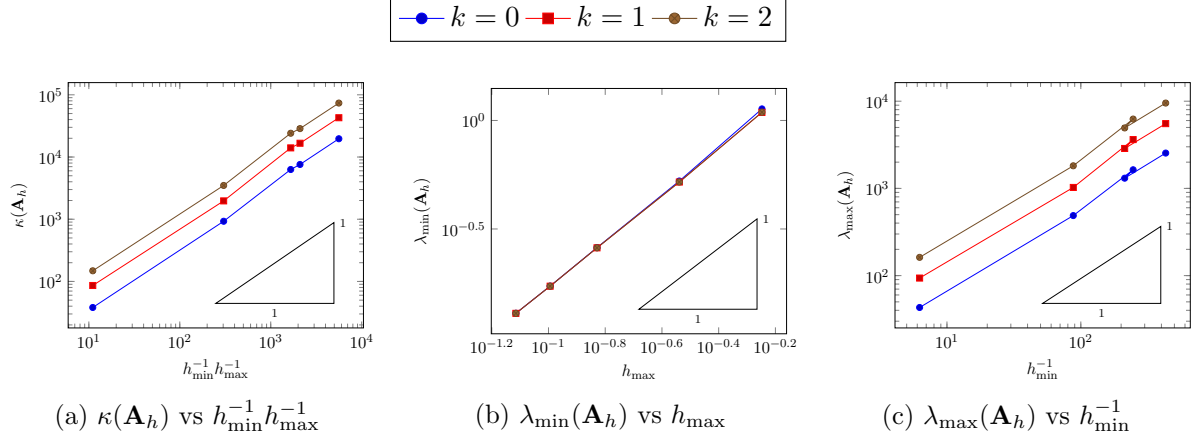


Figure 8: Circular meshes with sliver-cut elements aggregated

In Figure 9, results are plotted with both sliver-cut and small-cut elements aggregated. The condition number is one order of magnitude smaller than it was prior to aggregation, and scales as h^{-2} . Again, this is expected due to the meshes being quasi-uniform ($h = h_{\max} \sim h_{\min}$).

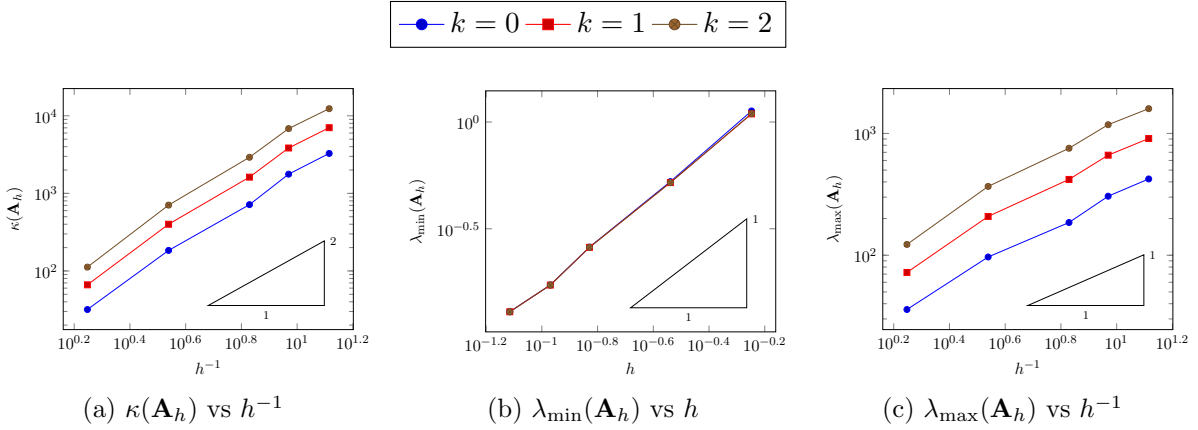


Figure 9: Circular meshes with sliver-cut and small-cut elements aggregated

5.3 Penta-diagonal meshes

We consider in this section a family of meshes with a penta-diagonal of elements being refined, with two large elements on each side, see Figure 10. The purpose of this test is to assess the accuracy of our estimates, and the robustness of the HHO condition number itself, when some large elements are neighbouring very small elements, all the while having an increasing number of faces. While testing on such extreme meshes is possibly contrived, the behaviour of the condition number illustrates that in some situations the estimates of Theorem 1 can be improved.

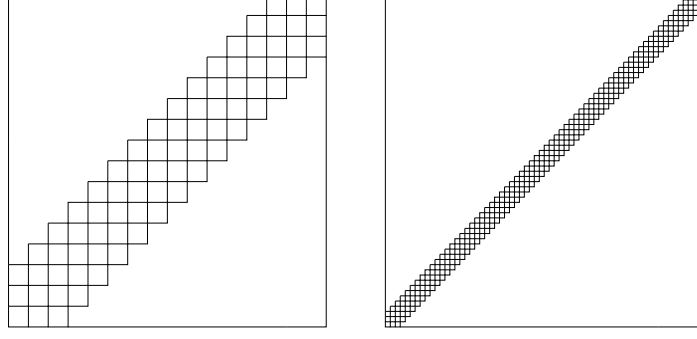


Figure 10: Penta-diagonal square meshes

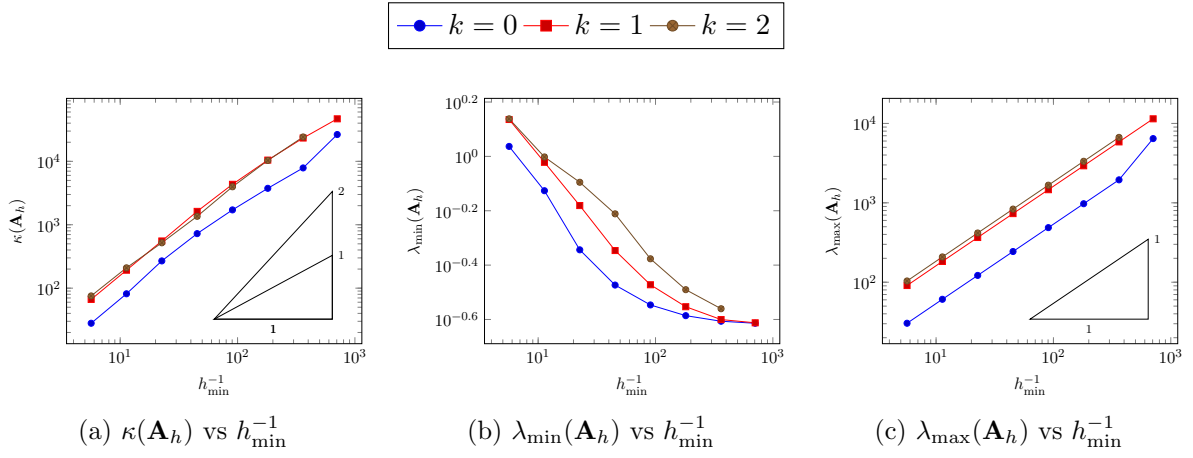


Figure 11: Penta-diagonal square meshes

The results presented in Figure 11 show a growth of the maximum eigenvalue as $\mathcal{O}(h_{\min}^{-1})$, which is consistent with the estimate (2.17b). Figure 11b however seems to indicate that, for this family of meshes, $\lambda_{\min}(\mathbf{A}_h)$ actually remains bounded below, which would indicate that the estimate (2.17a) is not optimal; it can actually be proved (see Lemma 11) that for these meshes the minimal eigenvalue indeed remains bounded below. As a consequence, the condition number $\kappa(\mathbf{A}_h)$ does not grow as $\mathcal{O}(h_{\min}^{-2})$ but as $\mathcal{O}(h_{\min}^{-1})$, which is illustrated in Figure 11a.

Lemma 11. *For the family of penta-diagonal meshes, it holds that $\lambda_{\min}(\mathbf{A}_h) \gtrsim c(l, k)^{-1}$.*

Proof. We first note that even if the penta-diagonal meshes do not satisfy Assumption 1 (due to the two large elements with “stairs” boundary), the analysis carried out in the previous sections still applies. Indeed, we can easily find uniform bi-Lipschitz mappings between each of these elements and a ball of size comparable to these elements, which ensures that the trace inequality (3.1) still holds; since all elements contain a ball of size comparable to their diameters, the other relevant inequalities (approximation properties of projectors, discrete inverse inequalities) also remain valid.

An inspection of the proof of Theorem 1 (see in particular (3.7)) reveals that the bound on $\lambda_{\min}(\mathbf{A}_h)$ is a direct consequence of (3.6). The result thus follows if we establish the following

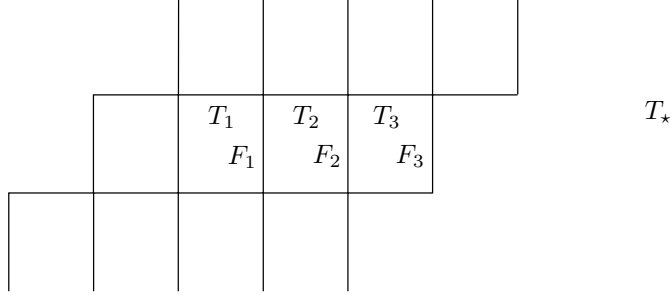


Figure 12: Illustration of the proof of Lemma 11.

improved version of this estimate: for all $\underline{v}_h \in \underline{U}_{h,0}^{k,l}$,

$$\sum_{T \in \mathcal{T}_h} \|v_{\partial T}\|_{\partial T}^2 \lesssim c(l, k) \|\underline{v}_h\|_{a,h}^2. \quad (5.1)$$

Let us take a face F in one of the small elements. Assuming for example that F is a vertical face, we can create a finite sequence of vertical faces ($F = F_1, F_2, \dots, F_r$) (with $r \leq 3$) such that F_r is a face of one of the two big elements in the mesh, say T_* ; see Figure 12 for an illustration.

Denoting by $(T_1, \dots, T_r, T_{r+1})$ with $T_{r+1} = T_*$ the elements encountered along the sequence (F_1, \dots, F_r) , we can then write

$$\begin{aligned} \|v_F\|_F &\leq \|v_{F_1} - v_{T_2}\|_F + \|v_{T_2} - \pi_{T_2}^{0,0} v_{T_2}\|_F + \|\pi_{T_2}^{0,0} v_{T_2}\|_{F_1} \\ &\lesssim h_{T_2}^{1/2} \|\underline{v}_{T_2}\|_{1,T_2} + \|\pi_{T_2}^{0,0} v_{T_2}\|_{F_2}, \end{aligned}$$

where we have introduced v_{T_2} and $\pi_{T_2}^{0,0} v_{T_2}$ in the first inequality, and used in the second line the definition of the semi-norm $\|\cdot\|_{1,T_2}$ together with the approximation properties of $\pi_{T_2}^{0,0}$ (which yield $\|v_{T_2} - \pi_{T_2}^{0,0} v_{T_2}\|_F \lesssim h_{T_2}^{1/2} \|\nabla v_{T_2}\|_{T_2} \leq h_{T_2}^{1/2} \|\underline{v}_{T_2}\|_{1,T_2}$), the fact that $\pi_{T_2}^{0,0} v_{T_2}$ is constant and $|F_1| = |F_2|$. Introducing then v_{F_2} in the last term and proceeding in a similar way, we obtain

$$\|v_F\|_F \lesssim h_{T_2}^{1/2} \|\underline{v}_{T_2}\|_{1,T_2} + \|v_{F_2}\|_{F_2}.$$

Iterating these estimates along the family (F_1, F_2, \dots, F_r) , squaring and using $r \leq 3$ and $h_{T_i} \lesssim 1$ we deduce that

$$\|v_F\|_F^2 \lesssim \sum_{i=2}^r \|\underline{v}_{T_i}\|_{1,T_i}^2 + \|v_{F_r}\|_{F_r}^2.$$

Summing this inequality over $F \in \mathcal{F}_T$ and then over the small elements T on the diagonal of the mesh, each of the small diagonal elements appear at most 3 times in the right-hand side, and the last boundary term is bounded above by $\|v_{\partial T_*}\|_{\partial T_*}^2$. This term can be estimated introducing v_{T_*} , using the definition of $\|\cdot\|_{1,T_*}$ and using a discrete trace inequality:

$$\|v_{\partial T_*}\|_{\partial T_*}^2 \lesssim \|v_{\partial T_*} - v_{T_*}\|_{\partial T_*}^2 + \|v_{T_*}\|_{\partial T_*}^2 \lesssim h_{T_*} \|v_{\partial T_*} - v_{T_*}\|_{1,T_*}^2 + h_{T_*}^{-1} \|v_{T_*}\|_{T_*}^2.$$

Using $h_{T_*} \gtrsim 1$, since T_* is one of the large elements whose diameter does not go to zero, and combining all these estimates leads to

$$\sum_{T \in \mathcal{T}_h} \|v_{\partial T}\|_{\partial T}^2 \lesssim \sum_{T \in \mathcal{T}_h} \|\underline{v}_T\|_{1,T}^2 + \|v_h\|_{\Omega}^2.$$

The estimate (5.1) follows from the discrete Poincaré inequality (3.3) and the leftmost bound in (2.8). \square

6 Conclusions

In this work, we have proved detailed eigenvalue and condition number bounds for the linear system matrix that arises from HHO discretisations of second-order linear elliptic problems. The analysis applies to general polytopal meshes and polynomial orders. It reveals the effect of small and highly distorted elements and faces on the conditioning of the linear system. Whereas highly distorted elements negatively impact condition numbers, faces shapes and sizes do not affect these bounds. With this information, we apply HHO methods on unfitted meshes. We combine simple background meshes, element intersection algorithms and an aggregation strategy to end up with well-posed HHO methods on unfitted meshes.

We carry out a detailed set of numerical experiments that are in agreement with the numerical analysis. First, we analyse the condition number as one coarsens polytopal meshes with many faces per element and arbitrarily small faces. Next, we show that the HHO method on aggregated unfitted meshes provides the expected condition number with respect to the mesh size. We also observe that the condition number of the algorithm is not affected by increasingly small cut elements. Finally, we consider a limit case with penta-diagonal squared meshes that motivates sharper condition number bounds for some specific mesh configurations.

Future work includes the combination of HHO methods with higher-order unfitted geometrical discretisations (curved boundaries) and the design of optimal and scalable preconditioners for these linear systems.

Acknowledgements

This work was partially supported by the Australian Government through the *Australian Research Council's* Discovery Projects funding scheme (grant number DP210103092).

References

- [1] Joubine Aghili, Daniele A Di Pietro, and Berardo Ruffini. An hp-hybrid high-order method for variable diffusion on general meshes. *Computational Methods in Applied Mathematics*, 17(3):359–376, 2017.
- [2] Santiago Badia, Eric Neiva, and Francesc Verdugo. Linking ghost penalty and aggregated unfitted methods, 2021.
- [3] Santiago Badia and Francesc Verdugo. Gridap: An extensible Finite Element toolbox in Julia. *Journal of Open Source Software*, 5(52):2520, 2020.
- [4] Santiago Badia, Francesc Verdugo, and Alberto F Martín. The aggregated unfitted finite element method for elliptic problems. *Computer Methods in Applied Mechanics and Engineering*, 336:533–553, 2018.
- [5] Laureço Beirão da Veiga, Franco Brezzi, Andrea Cangiani, Gianmarco Manzini, L Donatella Marini, and Alessandro Russo. Basic principles of virtual element methods. *Mathematical Models and Methods in Applied Sciences*, 23(01):199–214, 2013.
- [6] T Belytschko, N Moës, S Usui, and C Parimi. Arbitrary discontinuities in finite elements. *International Journal for Numerical Methods in Engineering*, 50(4):993–1013, 2001.
- [7] Erik Burman. Ghost penalty. *Comptes Rendus Mathématique*, 348(21-22):1217–1220, 2010.

- [8] Erik Burman, Matteo Cicuttin, Guillaume Delay, and Alexandre Ern. An unfitted hybrid high-order method with cell agglomeration for elliptic interface problems. *SIAM Journal on Scientific Computing*, 43(2):A859–A882, 2021.
- [9] Erik Burman, Susanne Claus, P Hansbo, M G Larson, and André Massing. CutFEM: Discretizing Geometry and Partial Differential Equations. *International Journal for Numerical Methods in Engineering*, 104(7):472–501, 2015.
- [10] Andrea Cangiani, Zhaonan Dong, and Emmanuil H Georgoulis. *hp-version discontinuous galerkin methods on essentially arbitrarily-shaped elements*. *arXiv preprint arXiv:1906.01715*, 2019.
- [11] Andrea Cangiani, Zhaonan Dong, Emmanuil H. Georgoulis, and Paul Houston. *hp-version discontinuous Galerkin methods on polygonal and polyhedral meshes*. SpringerBriefs in Mathematics. Springer, Cham, 2017.
- [12] B. Cockburn, O. Dubois, J. Gopalakrishnan, and S. Tan. Multigrid for an HDG method. *IMA Journal of Numerical Analysis*, 34(4):1386–1425, October 2013.
- [13] Bernardo Cockburn, Jayadeep Gopalakrishnan, and Raytcho Lazarov. Unified hybridization of discontinuous galerkin, mixed, and continuous galerkin methods for second order elliptic problems. *SIAM Journal on Numerical Analysis*, 47(2):1319–1365, January 2009.
- [14] F. de Prenter, C.V. Verhoosel, G.J. van Zwieten, and E.H. van Brummelen. Condition number analysis and preconditioning of the finite cell method. *Computer Methods in Applied Mechanics and Engineering*, 316:297–327, 2017. Special Issue on Isogeometric Analysis: Progress and Challenges.
- [15] Daniele Antonio Di Pietro and Jérôme Droniou. *The Hybrid High-Order Method for Polytopal Meshes: Design, Analysis, and Applications*, volume 19 of *Modeling, Simulation and Applications*. Springer International Publishing, <https://hal.archives-ouvertes.fr/hal-02151813>, 01 2020.
- [16] Daniele Antonio Di Pietro and Alexandre Ern. A hybrid high-order locking-free method for linear elasticity on general meshes. *Computer Methods in Applied Mechanics and Engineering*, 283:1–21, 2015.
- [17] Daniele Antonio Di Pietro, Alexandre Ern, and Simon Lemaire. An arbitrary-order and compact-stencil discretization of diffusion on general meshes based on local reconstruction operators. *Computational Methods in Applied Mathematics*, 14(4):461–472, 2014.
- [18] Jérôme Droniou. Hardcore.
- [19] Jérôme Droniou. Interplay between diffusion anisotropy and mesh skewness in hybrid high-order schemes. In *International Conference on Finite Volumes for Complex Applications*, pages 3–23. Springer, 2020.
- [20] Jérôme Droniou and Liam Yemm. Robust hybrid high-order method on polytopal meshes with small faces. *arXiv preprint arXiv:2102.06414*, 2021.
- [21] Alexandre Ern and Jean-Luc Guermond. Evaluation of the condition number in linear systems arising in finite element approximations. *ESAIM: Mathematical Modelling and Numerical Analysis*, 40(1):29–48, 2006.

- [22] Anita Hansbo and Peter Hansbo. An unfitted finite element method, based on Nitsche’s method, for elliptic interface problems. *Computer methods in applied mechanics and engineering*, 191(47-48):5537–5552, 2002.
- [23] August Johansson and Mats G. Larson. A high order discontinuous Galerkin Nitsche method for elliptic problems with fictitious boundary. *Numerische Mathematik*, 123(4):607–628, 2013.
- [24] Lorenzo Mascotto. Ill-conditioning in the virtual element method: Stabilizations and bases. *Numerical Methods for Partial Differential Equations*, 34(4):1258–1281, March 2018.
- [25] Eric Neiva and Santiago Badia. Robust and scalable h-adaptive aggregated unfitted finite elements for interface elliptic problems. *Computer Methods in Applied Mechanics and Engineering*, 380:113769, July 2021.
- [26] Dominik Schillinger and Martin Ruess. The Finite Cell Method: A review in the context of higher-order structural analysis of CAD and image-based geometric models. *Archives of Computational Methods in Engineering*, 22(3):391–455, 2015.
- [27] Francesc Verdugo, Eric Neiva, and Santiago Badia. GridapEmbedded. Version 0.7., October 2021. Available at <https://github.com/gridap/GridapEmbedded.jl>.